Ultrawideband Chirp Scaling Algorithm

Viet Thuy Vu, *Student Member, IEEE*, Thomas K. Sjögren, *Student Member, IEEE*, and Mats I. Pettersson, *Member, IEEE*

***Abstract*—A new version of chirp scaling (CS), the so-called ultrawideband (UWB) CS (UCS), is proposed in this letter. UCS aims at UWB synthetic aperture radar (SAR) systems utilizing large fractional bandwidth and wide antenna beamwidth associated with a wide integration angle. Furthermore, it is also valid for SAR systems with special characteristics such as ground-moving-target-indication SAR systems with a very high pulse repetition frequency.**

***Index Terms*—CARABAS-II, chirp scaling (CS), LORA, nonlinear FM, P-3, synthetic aperture radar (SAR), ultrawideband (UWB).**

I. Introduction

CHIRP scaling (CS) [1], [2] shows superiority to other synthetic aperture radar (SAR) imaging algorithms in terms of processing time for small scenes and/or low resolution. The algorithm does not require any interpolation and can be performed efficiently by employing fast Fourier transform (FFT) and complex multiplications. Imaging algorithms for ultrawideband (UWB) SAR, which support large size and high resolution, require a significant effort due to, e.g., the Stolt interpolation used in range migration (RM) [3]. UWB SAR here refers to systems utilizing large fractional bandwidth and wide antenna beamwidth which means that the bandwidth can be close to two times the center frequency and that the antenna pattern is almost isotropic. Based on this, there are some extreme difficulties in applying CS to UWB SAR. For example, the wide antenna beamwidth in the azimuth direction results in a pulse repetition frequency (PRF) higher than the processing PRF allowed by CS, and the large fractional bandwidth in the transmitted pulse requires a higher order Taylor expansion in CS (higher than the second order). Another difficulty may be found in large space-variant RM in the case where large illuminated SAR scenes supported by the wide antenna beamwidth in elevation are imaged. However, UWB SAR imaging algorithms without interpolation are still of great interest, and this letter derives a new version of CS which is able to process UWB SAR data.

II. CS and Its Inherent Limitations

In this section, we briefly describe CS and mention the inherent limitations of CS in UWB SAR. Similar to narrowband SAR systems, UWB SAR systems use the chirp signal. The mathematical representation of the phase of the received signal in a 2-D frequency domain is given by [1]

$$\Phi_r(f_t, f_\tau) = -\frac{4\pi r_0}{\mathrm{c}}\sqrt{(f_\tau + f_c)^2 - \left(\frac{f_t \mathrm{c}}{2v_{\mathrm{pl}}}\right)^2} - \frac{\pi f_\tau^2}{\kappa} \quad (1)$$

where r_0 is the minimum range to a target, c is the speed of light, v_{pl} is the speed of the SAR platform, κ is the chirp rate, and f_c is the radar center frequency. The range frequency f_τ is related to the sampling frequency, whereas the azimuth frequency f_t is related to the PRF. From a system designer's point of view, the PRF chosen must not be less than two times the maximum Doppler frequency f_D

$$f_D = \frac{2v_{\mathrm{pl}}}{\lambda_{\min}} \sin\left(\frac{\theta_{\max}}{2}\right) \quad (2)$$

where $\lambda_{\min}$ is the minimum signal wavelength and $\theta_{\max}$ is the maximum integration angle. A Taylor expansion to the second order of the square root term in (1) results in [1]

$$\Phi_r(f_t, f_\tau) \approx -\frac{4\pi r_0}{\lambda_c}\left(\beta + \frac{f_\tau}{\beta f_c} + \frac{(\beta^2 - 1) f_\tau^2}{2\beta^3 f_c^2}\right) - \frac{\pi f_\tau^2}{\kappa} \quad (3)$$

where

$$\beta = \sqrt{1 - \left(\frac{\lambda_c f_t}{2v_{\mathrm{pl}}}\right)^2} = \sqrt{1 - \chi^2}. \quad (4)$$

The maximum value of the quadratic term in (4), when $f_t = f_D$, can be represented by a function of the SAR system's parameters as

$$\chi(B_r, \theta_{\max}) \approx \left(1 + \frac{B_r}{2}\right) \sin\left(\frac{\theta_{\max}}{2}\right) \quad (5)$$

where $\theta_{\max}$ is the maximum integration angle and B_r is the fractional bandwidth defined by the ratio of the signal bandwidth B to the center frequency f_c. The fractional bandwidth is therefore limited by $0 < B_r < 2$.

Let us consider three well-known UWB SAR systems: CARABAS-II [4], LORA [5], and P-3 [6]. The main parameters of these systems are summarized in Table I. Fig. 1 shows the values of χ as a function of B_r and $\theta_{\max}$. The values of χ, which are calculated from the CARABAS-II, the LORA, and the P-3 parameters, are marked by solid black circles in Fig. 1. For CARABAS-II and LORA, χ is larger than 1 ($\chi \approx 1.31$ and $\chi \approx 1.35$), as shown in Fig. 1. This means that β can be complex at a number of azimuth frequencies. For this reason, neither CS nor its other versions work with CARABAS-II or LORA data. SAR systems with special characteristics such as

Manuscript received April 1, 2009; revised June 26, 2009 and August 14, 2009. Date of publication November 3, 2009; date of current version April 14, 2010.

The authors are with the Blekinge Institute of Technology, 372 25 Ronneby, Sweden (e-mail: viet.thuy.vu@bth.se).

Digital Object Identifier 10.1109/LGRS.2009.2033316

TABLE I
CARABAS-II, LORA, AND P-3 PARAMETERS

Parameter	CARABAS-II	LORA	P-3
f_{max}	90 MHz	800 MHz	900 MHz
f_{min}	20 MHz	200 MHz	215 MHz
v_{pl}	130 m/s	150 m/s	125 m/s
PRF	137 Hz	1545 Hz	333 Hz

a very high PRF for ground moving-target indication (GMTI) may also face the same challenge. However, P-3 does not suffer from this problem since χ is smaller than 1 ($\chi \approx 0.44$). This value is given by $B_r \approx 1.2$ and $\theta_{\max} \approx 32^\circ$. In general, CS and its versions are invalid for SAR systems with χ lying above the curve $\chi = 1$. A temporary solution for such a problem is to reduce the PRF [7] (e.g., by azimuth presuming or throwing away some of the pulses) to keep β real at all azimuth frequencies. However, the solution is likely to cause aliasing.

III. UCS

The concept of normalized relative speed (NRS) and its application in moving-target detection are presented in [8] and [9]. According to this concept, a moving target is focused, and a stationary target is defocused in the SAR formation process if the SAR platform is assumed to move with the relative speed which is the absolute value of the vector sum of the original platform velocity and the target velocity

$$\gamma = \sqrt{\frac{(v_{\rm pl} - v_\xi)^2 + v_\eta^2}{v_{\rm pl}^2}} \tag{6}$$

where v_ξ and v_η are the velocity components of the moving target. The idea behind UWB CS (UCS) is to assume a higher speed of the SAR platform in processing, i.e., scaling the speed of the SAR platform with NRS $\gamma > 1$, to keep β real at all azimuth frequencies. Defocusing caused by NRS will be compensated in the phase functions of UCS. With this proposal, the term β_γ can be defined as

$$\beta_\gamma = \sqrt{1 - \left(\frac{\lambda_c f_t}{2\gamma v_{\rm pl}}\right)^2}. \tag{7}$$

Due to the large fractional bandwidths utilized by UWB SAR systems, the Taylor expansion to quadratic terms in CS may be insufficient. In [10], UWB SAR data are successfully processed with the nonlinear CS (NCS) algorithm utilizing a Taylor expansion up to cubic terms. In UCS, we propose to use a Taylor expansion up to quartic terms. With this expansion, (3) can be rewritten with the term β_γ defined in (7) as

$$\Phi_r(f_t, f_\tau) \approx \phi_0(f_t) + \phi_1(f_t) f_\tau + \phi_2(f_t) f_\tau^2 + \phi_3(f_t) f_\tau^3 + \phi_4(f_t) f_\tau^4 \tag{8}$$

where

$$\phi_0(f_t) = -\frac{4\pi r_0 \beta_\gamma}{\lambda_c}\left(1 + \frac{8\zeta_\gamma - 4\zeta_\gamma^2 + 4\zeta_\gamma^3 - 5\zeta_\gamma^4}{8}\right) \tag{9}$$

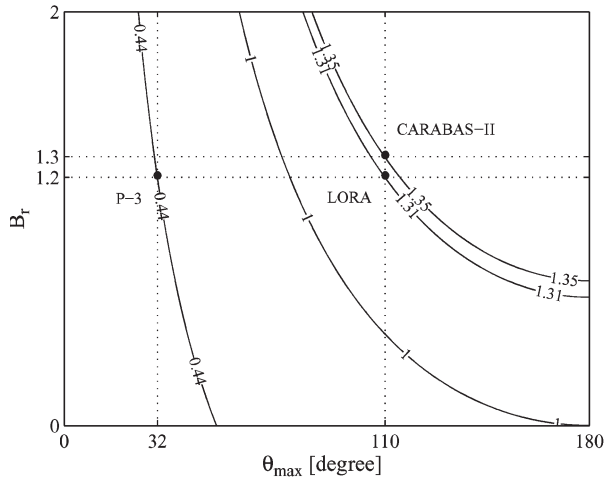

Fig. 1. Values of χ as a function of B_r and $\theta_{\max}$. The solid black circles denote χ calculated from CARABAS-II, LORA, and P-3 system parameters. CS is valid for SAR systems with χ lying below the curve $\chi = 1$. UCS is aimed at SAR systems with χ lying above the curve $\chi = 1$.

$$\phi_1(f_t) = -\frac{4\pi r_0}{\rm c}\left(\frac{1}{\beta_\gamma} - \frac{2\zeta_\gamma - 3\zeta_\gamma^2 + 5\zeta_\gamma^3}{2\beta_\gamma}\right) \tag{10}$$

$$\phi_2(f_t) = -\frac{\pi}{\kappa} - \frac{4\pi r_0}{{\rm c} f_c}\left(\frac{\beta_\gamma^2 - 1}{2\beta_\gamma^3} - \frac{2\zeta_\gamma - 3\zeta_\gamma^2 + 5\zeta_\gamma^3}{4\beta_\gamma} + \frac{6\zeta_\gamma - 15\zeta_\gamma^2}{4\beta_\gamma^3}\right). \tag{11}$$

$\phi_3(f_t)$ and $\phi_4(f_t)$ are given in Appendix A. The term ζ_γ in (9)–(11) is given by

$$\zeta_\gamma = \frac{(1-\gamma^2)\left(1-\beta_\gamma^2\right)}{2\beta_\gamma^2}. \tag{12}$$

Wide integration angles in UWB SAR and large illuminated SAR scenes, which are synonymous with large space-variant RM, can be handled by the nonlinear FM filtering method [2], i.e., NCS. Due to the consideration of the quartic terms in the Taylor expansion, the extra phase filter $H_0(f_t, f_\tau)$ in [2] should be modified to

$$H_0(f_t, f_\tau) = \exp\left[i\pi Y(f_t) f_\tau^3 + i\pi Z(f_t) f_\tau^4\right] \tag{13}$$

where $Y(f_t)$ and $Z(f_t)$ are the azimuth frequency varying phase filter coefficients. Under certain conditions [2], the linear FM can be assumed to be dominant. An inverse Fourier transform in range after this filtering step is approximated by

$$\Phi_r(f_t, \tau) \approx -\frac{4\pi r_0 \beta_\gamma}{\lambda_c}\left(1 + \frac{8\zeta_\gamma - 4\zeta_\gamma^2 + 4\zeta_\gamma^3 - 5\zeta_\gamma^4}{8}\right) + \pi K_\gamma\left[\tau - \frac{2r_0}{\rm c}(1+\xi_\gamma)\right]^2 + \pi Y_\gamma(f_t) K_\gamma^3\left[\tau - \frac{2r_0}{\rm c}(1+\xi_\gamma)\right]^3 + \pi Z_\gamma(f_t) K_\gamma^4\left[\tau - \frac{2r_0}{\rm c}(1+\xi_\gamma)\right]^4 \tag{14}$$

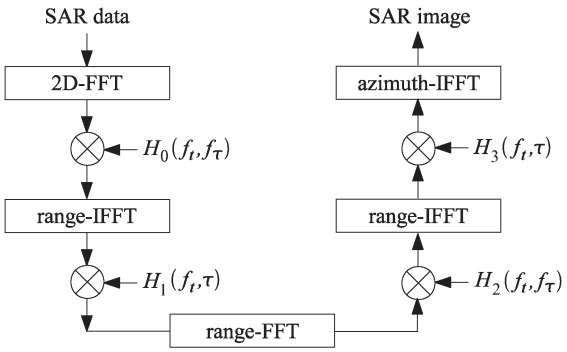

Fig. 2. Block diagram of UCS.

where K_γ is the range frequency rate and determined by

$$\frac{1}{K_\gamma} = \frac{1}{\kappa} + \frac{2r_0}{\mathrm{c}f_c}\left(\frac{\beta_\gamma^2 - 1}{\beta_\gamma^3} - \frac{2\zeta_\gamma - 3\zeta_\gamma^2 + 5\zeta_\gamma^3}{2\beta_\gamma} + \frac{6\zeta_\gamma - 15\zeta_\gamma^2}{2\beta_\gamma^3}\right) \tag{15}$$

$$\xi_\gamma = \frac{1}{\beta_\gamma} - 1 - \frac{2\zeta_\gamma - 3\zeta_\gamma^2 + 5\zeta_\gamma^3}{2\beta_\gamma} \tag{16}$$

$$Y_\gamma(f_t) = Y(f_t) + \phi_3(f_t) \tag{17}$$

$$Z_\gamma(f_t) = Z(f_t) + \phi_4(f_t). \tag{18}$$

If the range frequency rate at the reference range r_{ref} is denoted by K_{ref}, another Taylor expansion up to quadratic terms for the range frequency rate K_γ results in

$$K_\gamma \approx K_{\mathrm{ref}}\left[1 - K_s R_\gamma + (K_s R_\gamma)^2\right] \tag{19}$$

where

$$K_s = \frac{K_{\mathrm{ref}}}{f_c}\left[1 - \frac{2 - 6\zeta_\gamma + 15\zeta_\gamma^2}{\beta_\gamma^2\left(2 - 2\zeta_\gamma + 3\zeta_\gamma^2 - 5\zeta_\gamma^3\right)}\right] \tag{20}$$

$$R_\gamma = \frac{2(r_0 - r_{\mathrm{ref}})}{\mathrm{c}}(\xi_\gamma + 1). \tag{21}$$

This means that K_γ is assumed to vary not only linearly but also quadratically with R_γ. The azimuth frequency varying phase filter coefficients are retrieved from (17) and (18) where $Y_\gamma(f_t)$ and $Z_\gamma(f_t)$ are shown to be

$$Y_\gamma(f_t) = -\frac{K_s(1 + 2\xi_\gamma)}{3K_{\mathrm{ref}}^2\xi_\gamma} \tag{22}$$

$$Z_\gamma(f_t) = \frac{K_s^2\left(3 + 10\xi_\gamma + 10\xi_\gamma^2\right)}{12K_{\mathrm{ref}}^3\xi_\gamma^2}. \tag{23}$$

The next processing steps of UCS are similar to CS. The block diagram of UCS is shown in Fig. 2. Phase functions of CS $H_1(f_t,\tau)$, range compression $H_2(f_t,f_\tau)$, and residual phase correction $H_3(f_t,f_\tau)$, which include the NRS defocusing compensation, are given by

$$\begin{aligned} H_1(f_t,\tau) &= \exp\left\{i\pi K_{\mathrm{ref}}\xi_\gamma\left[\tau - \frac{2r_{\mathrm{ref}}}{\mathrm{c}}\right]^2\right\} \\ &\quad\cdot\exp\left\{-\frac{i\pi K_s\xi_\gamma}{3}\left[\tau - \frac{2r_{\mathrm{ref}}}{\mathrm{c}}\right]^3\right\} \\ &\quad\cdot\exp\left\{\frac{i\pi K_s^2 K_{\mathrm{ref}}(1 + 4\xi_\gamma)}{12}\left[\tau - \frac{2r_{\mathrm{ref}}}{\mathrm{c}}\right]^4\right\} \end{aligned} \tag{24}$$

$$\begin{aligned} H_2(f_t,f_\tau) &= \exp\left\{\frac{i4\pi f_\tau r_{\mathrm{ref}}\xi_\gamma}{\mathrm{c}} + \frac{i\pi f_\tau^2}{K_{\mathrm{ref}}(1 + \xi_\gamma)}\right\} \\ &\quad\cdot\exp\left\{\frac{i\pi K_s f_\tau^3}{3K_{\mathrm{ref}}^2\xi_\gamma(1 + \xi_\gamma)} - \frac{i\pi K_s^2(3 + 4\xi_\gamma)f_\tau^4}{12K_{\mathrm{ref}}^3\xi_\gamma^2(1 + \xi_\gamma)^2}\right\} \end{aligned} \tag{25}$$

$$\begin{aligned} H_3(f_t,\tau) &= \exp\left\{\frac{i4\pi f_c r_0\beta_\gamma}{\mathrm{c}}\left(1 + \frac{8\zeta_\gamma - 4\zeta_\gamma^2 + 4\zeta_\gamma^3 - 5\zeta_\gamma^4}{8}\right)\right\} \\ &\quad\cdot\exp\left\{-i\pi K_{\mathrm{ref}}(1 + \xi_\gamma)\xi_\gamma\left[\frac{2(r_0 - r_{\mathrm{ref}})}{\mathrm{c}}\right]^2\right\} \\ &\quad\cdot\exp\left\{\frac{i\pi K_{\mathrm{ref}}K_s(1 + \xi_\gamma)^2\xi_\gamma}{3}\left[\frac{2(r_0 - r_{\mathrm{ref}})}{\mathrm{c}}\right]^3\right\} \\ &\quad\cdot\exp\left\{\frac{i\pi K_{\mathrm{ref}}K_s^2(1 + \xi_\gamma)^2}{12\left(1 + 2\xi_\gamma - 14\xi_\gamma^2\right)^{-1}}\left[\frac{2(r_0 - r_{\mathrm{ref}})}{\mathrm{c}}\right]^4\right\} \end{aligned} \tag{26}$$

respectively. Processing UWB SAR data with γ and then compensating the defocusing in the reference functions can also be applied to the original CS or its other versions, e.g., the reference functions of NCS with extensions for UWB SAR are found in $H_1(f_t,\tau)$, $H_2(f_t,f_\tau)$, and $H_3(f_t,\tau)$ without the quartic terms.

A critical question is how γ is selected. An obvious condition for γ to ensure that β_γ is real can be determined from (7) directly as

$$\gamma > \frac{\lambda_c}{4\Delta L} \tag{27}$$

where ΔL is the along-track space between two adjacent SAR platform positions. Another condition for γ is connected to the assumption of the Taylor expansion

$$\left|2\beta_\gamma^2\zeta_\gamma + 2\frac{f_\tau}{\beta_\gamma^2 f_c} + \frac{f_\tau^2}{\beta_\gamma^2 f_c^2}\right| < 1 \tag{28}$$

and the following is expected:

$$\left|(1 - \gamma^2)\left(1 - \beta_\gamma^2\right)\right| \ll 1 \tag{29}$$

or

$$\gamma^2 \gg 0.5. \tag{30}$$

Equations (27) and (30) result in many possible selections for γ. In theory, the defocusing caused by γ in a SAR image can be compensated completely. However, to minimize the possible

effects of γ to the unconsidered terms in the Taylor expansion, $\zeta_\gamma \approx 0$ should hold. γ should be set as small as possible, while being sufficiently large to keep β_γ real.

Let us have a look at (28). For radar signals with extremely large fractional bandwidth ($B_r > 1$), some range frequencies violate the assumption of the Taylor expansion. A limit of fractional bandwidth (applying to all CS versions) to fulfill the assumption of the Taylor expansion at all range frequencies and therefore result in high SAR image quality is found by

$$B_r^2 + 2B_r + \chi^2\left(B_r, \theta_{\max}\right) < 1 \tag{31}$$

and can be roughly given by

$$B_r < 0.4 \tag{32}$$

Processing UWB SAR data having $B_r > 1$ without interpolation by UCS therefore suffers from undesired effects. The phase error is one example which is caused by large range frequencies. The phase error causes a reduction in SAR image quality. This reduction is evaluated by the focusing ability of UCS and presented in the next section.

IV. Simulation and Evaluation

In this section, UCS is tested with the CARABAS-II simulated data. The SAR scene in this simulation includes five different point targets implying different RMs. The minimum range to the middle point target is 4500 m. From a user's point of view, it is not always required to process the full aperture which, in this case, refers to an integration angle of $\theta_{\max} = 110^\circ$. To demonstrate the validity of UCS for UWB SAR, the SAR scene is processed by UCS with $\theta = 15^\circ$ (narrow) and $\theta = 65^\circ$ (wide), i.e., using a part of the full aperture. The space between two adjacent SAR platform positions is constant $\Delta L = 0.9375$ m, i.e., constant $v_{\rm pl}$. An NRS $\gamma \approx 1.6$ is selected for UCS based on (27). Fig. 3(a) and (c) shows the imaged scene. The extracted impulse responses in SAR imaging (IR-SAR) are shown in Fig. 3(b) and (d).

The simulation illustrated the validity of UCS for UWB SAR systems in general and for CARABAS-II in particular. The defocusing which is caused by NRS connected to the term β_γ in (7) is compensated in the reference functions (24)–(26) and does not appear in the SAR images. At small integration angles and for small illuminated SAR scenes, we may not need to consider the cubic and quartic terms in the Taylor expansion. However, we still need to scale the speed of the platform with γ to keep β_γ real.

To achieve a better evaluation of UCS, we apply two main criteria: accuracy and processing time. To evaluate the accuracy of UCS, we measure the spatial resolutions (RES) and differential resolutions (DRES) [11] at different integration angles. The references for the DRES measurements are the azimuth and range resolutions obtained with RM [3]. The RM algorithm has been proved to be suitable for UWB SAR data processing in [7] and applied to the moving-target detection by focusing technique in [8]. The measured results are shown in Fig. 4. A range of integration angles from 5° to 70° has been used in these measurements. The measured results of DRES in Fig. 4(b) show the loss in spatial resolutions of UCS with respect to RM. The results show the ability of UCS to handle azimuth

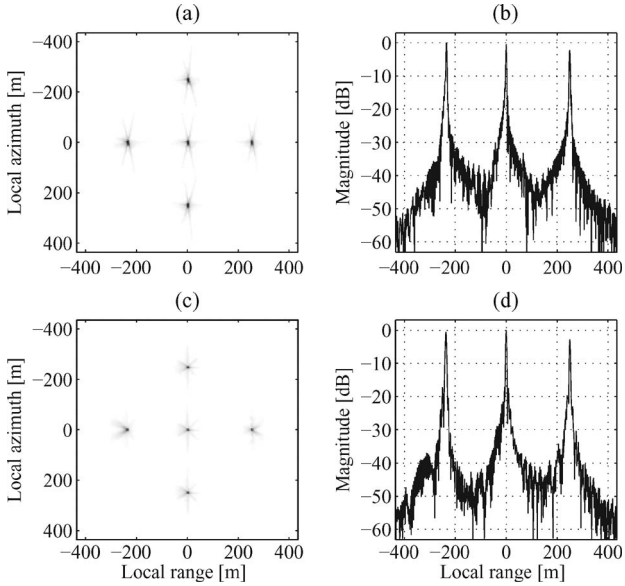

Fig. 3. SAR scene of five point targets imaged by UCS with different values of θ and the extracted SAR image in the range direction. The measured integrated sidelobe ratio (ISLR) and peak sidelobe ratio (PSLR) on the range vectors of the middle point target are about -13 and -18 dB, respectively, at $\theta = 15^\circ$ and 65°. (a) Imaged scene with $\theta = 15^\circ$. (b) Extracted range at $\theta = 15^\circ$. (c) Imaged scene with $\theta = 65^\circ$. (d) Extracted range at $\theta = 65^\circ$.

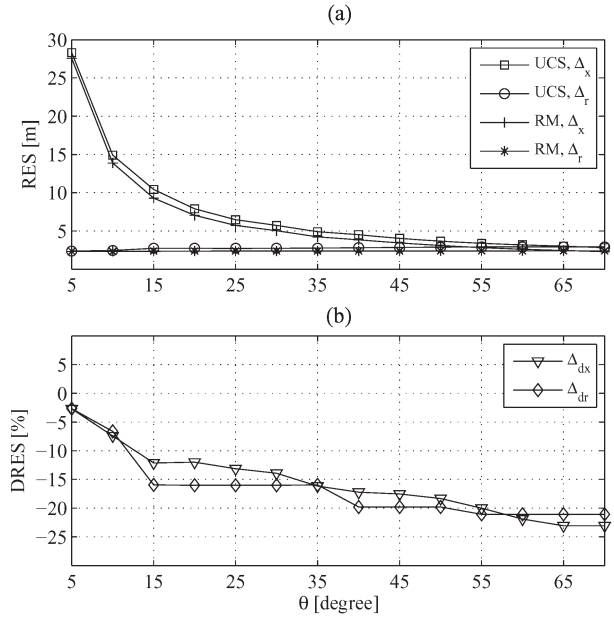

Fig. 4. RES measurements in azimuth Δ_x and in range Δ_r (-3 dB beamwidths) given by UCS and DRES measurements $\Delta_{\rm dx}$ and $\Delta_{\rm dr}$ where the spatial equations obtained with RM are references. The DRES measurements present the loss in spatial resolutions. (a) RES. (b) DRES.

focusing. However, this ability is reduced with the increase of the integration angle. This can be explained by the phase errors caused by the approximations as well as the effects of NRS on the unconsidered terms in both (8) and (19). In addition, the conditions (the small cubic and quartic terms) to obtain (14) may not be totally fulfilled.

The processing time of an imaging algorithm is always proportional to the required number of operations. As shown in Fig. 2, UCS requires an additional 2D-FFT and a complex multiplication for the phase filter $H_0(f_t, f_\tau)$ compared to CS. If

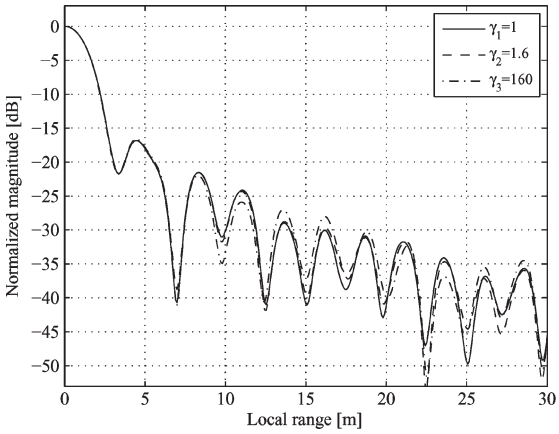

Fig. 5. Plots of a part of the SAR image in the range direction of the middle point target which are defocused by different γ values and then focused by the reference functions of UCS. Errors caused by γ are almost negligible, even in the extreme case where $\gamma_3 = 160$.

FFT is based on the radix-2 approach, the number of operations required by UCS can be roughly estimated by

$$N_x \times N_r \times [3 \times 5 \times \log_2(N_x \times N_r) + 4 \times 6] \tag{33}$$

where N_x and N_r are the numbers of the azimuth and range data, respectively. For RM, the number of operations is counted by one 2D-FFT, one Stolt interpolation, one complex multiplication (exponential terms), and one 2D-IFFT [3]

$$N_x \times N_r \times [2 \times 5 \times \log_2(N_x \times N_r) + N_{\text{int}} + 6] \tag{34}$$

where N_{int} denotes the number of operations needed to interpolate one data sample and depends on the selection of the interpolator. The Stolt interpolation normally leads to the high computational complexity of RM.

In the next simulation, we investigate effects of the selection of γ on UCS. Different values of γ, for example, $\gamma_1 = 1$, $\gamma_2 = 1.6$, and in an extreme case, $\gamma_3 = 160$, are used in this simulation. To ensure that UCS works with $\gamma_1 = 1$, we consider another SAR system with $\chi = 0.44$, i.e., the value of χ corresponds to P-3. For simplification, we still use the same center frequency of CARABAS-II, i.e., $f_c = 55$ MHz.

A similar SAR scene to the previous test is used. However, we concentrate only on the middle point target for evaluation purposes. Fig. 5 shows the IR-SAR of the middle point target which is defocused by different γ values and then focused by the reference functions of UCS. The simulation results indicate that γ does not strongly affect the final SAR images; in other words, the phase error caused by γ can be negligible. However, the selection of $\gamma \approx 1$ causes less effects than $\gamma \gg 1$.

V. Conclusion

In this letter, a new version of CS aimed at UWB SAR systems, so-called UCS, has been proposed. UCS is developed on CS with considerations of NRS to assume a higher platform speed in processing, the Taylor expansion up to the quartic terms, and the nonlinear FM filtering method to handle space-variant RM. The scaling platform speed in UCS is always required, even at small θ, when processing data collected by SAR systems with χ lying above the curve $\chi = 1$. As shown in the simulations, this scaling does not cause any significant effect to the final SAR images. For this reason, UCS is totally valid for SAR-GMTI systems with a very high PRF. The algorithm has been tested successfully with the simulated UWB SAR data to image a large SAR scene.

Appendix A

The terms $\phi_3(f_t)$ and $\phi_4(f_t)$ are given by

$$\phi_3(f_t) = \frac{4\pi r_0}{\mathrm{c} f_c^2}\left(\frac{\beta_\gamma^2 - 1}{2\beta_\gamma^5} - \frac{6\zeta_\gamma - 15\zeta_\gamma^2}{4\beta_\gamma^3} + \frac{5\zeta_\gamma}{2\beta_\gamma^5}\right) \tag{A1}$$

$$\phi_4(f_t) = \frac{4\pi r_0}{\mathrm{c} f_c^3}\left(\frac{\beta_\gamma^4 - 6\beta_\gamma^2 + 5}{8\beta_\gamma^7} - \frac{6\zeta_\gamma - 15\zeta_\gamma^2}{16\beta_\gamma^3} + \frac{15\zeta_\gamma}{4\beta_\gamma^5}\right). \tag{A2}$$

In practice, the Taylor expansion (8) only needs to be considered up to the quadratic terms, and the higher order terms $\phi_3(f_t)$ and $\phi_4(f_t)$ can be included in an extra phase filter $H_0'(f_t, f_\tau)$

$$H_0'(f_t, f_\tau) = \exp\left[i\pi Y_\gamma(f_t) f_\tau^3 + i\pi Z_\gamma(f_t) f_\tau^4\right]. \tag{A3}$$

Acknowledgment

The authors would like to thank the KK-Foundation for making this research project possible and the Swedish Defence Research Agency, Saab Bofors Dynamics, Saab Microwave Systems, and RUAG Space for their support.

References

[1] R. K. Raney, H. Runge, R. Bamler, I. G. Cumming, and F. H. Wong, "Precision SAR processing using chirp scaling," *IEEE Trans. Geosci. Remote Sens.*, vol. 32, no. 4, pp. 786–799, Jul. 1994.

[2] G. W. Davidson, I. G. Cumming, and M. R. Ito, "A chirp scaling approach for processing squint mode SAR data," *IEEE Trans. Aerosp. Electron. Syst.*, vol. 32, no. 1, pp. 121–133, Jan. 1996.

[3] C. Cafforio, C. Prati, and F. Rocca, "SAR data focusing using seismic migration techniques," *IEEE Trans. Aerosp. Electron. Syst.*, vol. 27, no. 2, pp. 194–207, Mar. 1991.

[4] A. Gustavsson, L. M. H. Ulander, B. H. Flood, P.-O. Frölind, H. Hellsten, T. Jonsson, B. Larsson, and G. Stenstrom, "Development and operation of an airborne VHF SAR system—lessons learned," in *Proc. IEEE IGARSS*, Seattle, WA, Jul. 1998, vol. 1, pp. 458–462.

[5] L. M. H. Ulander and H. Hellsten, "Low-frequency ultrawideband array-antenna SAR for stationary and moving target imaging," in *Proc. SPIE—Radar Sensing Technology IV*, Orlando, FL, Apr. 1999, vol. 3704, pp. 149–158.

[6] D. R. Sheen, C. M. Strawitch, and T. B. Lewis, "UHF wideband SAR design and preliminary results," in *Proc. IEEE IGARSS*, Pasadena, CA, Aug. 1994, vol. 1, pp. 289–291.

[7] V. T. Vu, T. K. Sjögren, and M. I. Pettersson, "A comparison between fast factorized backprojection and frequency-domain algorithms in UWB low frequency SAR," in *Proc. IEEE IGARSS*, Boston, MA, Jul. 2008, pp. IV-1284–IV-1287.

[8] V. T. Vu, T. K. Sjögren, and M. I. Pettersson, "Moving target detection by focusing for frequency domain algorithms in UWB low frequency SAR," in *Proc. IEEE IGARSS*, Boston, MA, Jul. 2008, pp. I-161–I-164.

[9] V. T. Vu, T. K. Sjögren, M. I. Pettersson, L. M. H. Ulander, and A. Gustavsson, "Moving targets detection by focusing in UWB SAR—Theory and experimental results," *IEEE Trans. Geosci. Remote Sens.*, to be published.

[10] J. Wang, G. Xue, Z. Zhou, and Q. Song, "A new subaperture nonlinear chirp scaling algorithm for real-time UWB-SAR imaging," in *Proc. CIE Int. Conf. Radar*, Shanghai, China, Oct. 2006, pp. 1–4.

[11] V. T. Vu, T. K. Sjögren, M. I. Pettersson, and A. Gustavsson, "Definition on SAR image quality measurements for UWB SAR," in *Proc. SPIE—Image and Signal Processing for Remote Sensing XIV*, Cardiff, U.K., Sep. 2008, vol. 7109, pp. 710 91A-1–710 91A-9.